NANO LETTERS

Letter

pubs.acs.org/NanoLett

Interface Engineering of Domain Structures in $BiFeO_3$ Thin Films

Deyang Chen,[*,†,‡,§,●] Zuhuang Chen,[‡] Qian He,[∥] James D. Clarkson,[‡] Claudy R. Serrao,[▽] Ajay K. Yadav,[‡] Mark E. Nowakowski,[▽] Zhen Fan,[†] Long You,[⊥] Xingsen Gao,[*,†] Dechang Zeng,[*,§] Lang Chen,[#] Albina Y. Borisevich,[∥] Sayeef Salahuddin,[▽] Jun-Ming Liu,[†,¶] and Jeffrey Bokor[▽]

[†]Institute for Advanced Materials and Guangdong Provincial Key Laboratory of Quantum Engineering and Quantum Materials, South China Normal University, Guangzhou 510006, China

[‡]Department of Materials Science and Engineering, University of California, Berkeley, Berkeley, California 94720, United States

[§]School of Materials Science and Engineering, South China University of Technology, Guangzhou 510640, China

[∥]Materials Science and Technology Division, Oak Ridge National Laboratory, Oak Ridge, Tennessee 37831, United States

[⊥]School of Optical and Electronic Information, Huazhong University of Science and Technology, Wuhan 430074, China

[#]Department of Physics, South University of Science and Technology of China, Shenzhen 518055, China

[▽]Department of Electrical Engineering and Computer Sciences, University of California Berkeley, Berkeley, California 94720, United States

[¶]Laboratory of Solid State Microstructures and Innovation Center of Advanced Microstructures, Nanjing University, Nanjing 210093, China

[●]Department of Physics, University of California Berkeley, Berkeley, California 94720, United States

S *Supporting Information*

ABSTRACT: A wealth of fascinating phenomena have been discovered at the $BiFeO_3$ domain walls, examples such as domain wall conductivity, photovoltaic effects, and magnetoelectric coupling. Thus, the ability to precisely control the domain structures and accurately study their switching behaviors is critical to realize the next generation of novel devices based on domain wall functionalities. In this work, the introduction of a dielectric layer leads to the tunability of the depolarization field both in the multilayers and superlattices, which provides a novel approach to control the domain patterns of $BiFeO_3$ films. Moreover, we are able to study the switching behavior of the first time obtained periodic 109° stripe domains with a thick bottom electrode. Besides, the precise controlling of pure 71° and 109° periodic stripe domain walls enable us to make a clear demonstration that the exchange bias in the ferromagnet/$BiFeO_3$ system originates from 109° domain walls. Our findings provide future directions to study the room temperature electric field control of exchange bias and open a new pathway to explore the room temperature multiferroic vortices in the $BiFeO_3$ system.

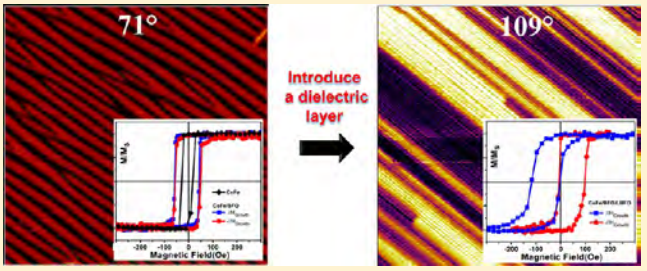

KEYWORDS: *$BiFeO_3$, multiferroic, depolarization field, domain wall, exchange bias, superlattices*

The atomic-scale growth techniques of oxide heterostructures provide a wealth of splendid possibilities for creating novel states at their interfaces,[1−3] leading to a large number of emergent physical phenomena and functionalities as a consequence of the complex interplay of spin, charge, orbital, and lattice degrees of freedom.[4−8] In ferroelectric materials, interfaces play a pivotal role in the formation of various domain structures, such as the observation of flux-closure polar domains in the ferroelectric/paraelectric $PbTiO_3/SrTiO_3$ multilayer films.[9] Moreover, our recent study[10] demonstrated that, due to the interplay among strain, depolarization field, and gradient energies, topological ferroelectric vortices can be produced in $PbTiO_3/SrTiO_3$ superlattices. Interestingly, the domain structures can be engineered from a_1/a_2 domains to vortex−antivortex structures and then to classical flux-closure domain structures with the increase of the superlattice period, strongly depending on the interface effects of the depolarization field. Besides, extensive efforts have recently been focused on the control of domain structures through the tuning of depolarization field in $BaTiO_3$, $PbTiO_3$, and $Pb(Zr,Ti)O_3$ thin films.[11−14] By inserting a dielectric $SrTiO_3$ layer under the ferroelectric layer, Lichtensteiger et al.[13] and Liu et al.[14] showed that the domain configuration evolved from monodomain to polydomain as the thickness of $SrTiO_3$ space layer increases, in $PbTiO_3$ and $Pb(Zr,Ti)O_3$ thin films, respectively. Based on the prior work, here we are motivated to explore the interface

Received: October 28, 2016
Revised: December 3, 2016
Published: December 7, 2016

DOI: 10.1021/acs.nanolett.6b04512
Nano Lett. 2017, 17, 486−493

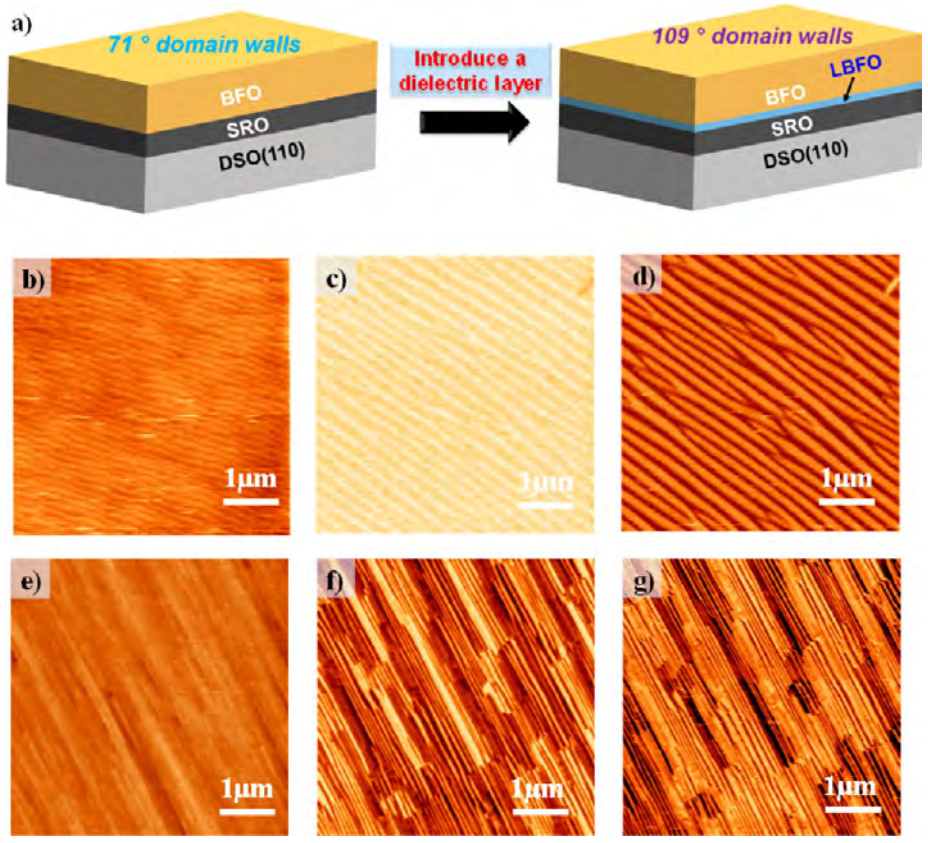

Figure 1. Domain "switch" by inserting a dielectric layer. (a) Schematics of the experimental design to induce the domain structure evolution by introducing a dielectric layer. (b) Topography, (c) out-of-plane PFM image, and (d) in-plane PFM image demonstrate the periodic 71° stripe domain structure in BFO/SRO/DSO. (e) Topography, (f) out-of-plane PFM image, and (g) in-plane PFM image reveal the periodic 109° stripe domain structure in BFO/LBFO/SRO/DSO.

engineering of domain structure evolution in $BiFeO_3$ (BFO) thin films by introducing a dielectric layer.

BFO is a room-temperature multiferroic[15] with a rhombohedral structure, giving rise to three possible domain walls including 71°, 109°, and 180° types.[16] A large number of fascinating phenomena and functionalities have been discovered at the domain walls in BFO thin films, examples such as domain wall conductivity,[17,18] photovoltaic effects,[19−22] magnetoelectric coupling,[23−26] enhanced magnetism,[27] and magnetotransport properties,[28] enabling a wide variety of potential device applications for electronics, photonics, and spintronics.[29−32] Therefore, the ability to precisely control the domain structures (especially for the periodic domain structures) in BFO thin films is critical to enable the study of these exotic properties and the design of next generation of novel devices based on the domain wall functionalities.

Periodically ordered 71°, 109°, and 180° stripe domains have been obtained through tuning of the electrostatic boundary conditions.[33−35] Chu et al.[34] showed that periodic 109° stripe domains can be produced in BFO thin films without or with a very thin (<5 nm) $SrRuO_3$ (SRO) bottom electrode layer, while periodic 71° domain structures would form on thicker SRO (>25 nm), due to the screening effects from metal (SRO)−ferroelectric (BFO) interfaces. It has been shown that exchange coupling between a ferromagnetic layer and multiferroic BFO layer enables an exchange enhancement of the ferromagnet with BFO 71° domain walls or both an exchange enhancement and exchange bias of the ferromagnet with mosaic domain structures (including a large fraction of 109° domain walls),[36] providing the possibility of controlling ferromagnetism with an electric field, which has exciting application potentials in the low-energy-consumption, nonvolatile magnetoelectronic memory devices. Indeed, the precise control of periodic 71° stripe domains on thick SRO bottom electrode (these domains are reversible and controllable by electric field) has promoted several seminal works on electric field control of magnetism in the ferromagnet/multiferroic BFO system.[23,24,26] However, the periodic 109° stripe domains can only exist without (or with ultrathin) SRO bottom electrode (these domains are typically unstable or unresponsive under an applied electric field),[34] inhibiting not only the study of switching behavior of 109° domains, but the potential to control the exchange bias using an electric field.

In this work, we demonstrate a depolarization field induced domain structure evolution in BFO/$La_xBi_{1-x}FeO_3$ (BFO/LBFO) multilayers and extend this discovery to BFO/LBFO superlattices. $La_{0.25}Bi_{0.75}FeO_3$ (LBFO), unlike the pure BFO with ferroelectric rhombohedral phase, possesses an equilibrium nonferroelectric orthorhombic structure.[37,38] We introduce LBFO as a dielectric layer between the bottom electrode (SRO) and the ferroelectric BFO layer to investigate the interface effects of depolarization field driven domain structure evolution. The "homoepitaxial" growth of BFO on LBFO enables us to grow high-quality multilayers and superlattices, which is another reason we use LBFO as the dielectric layer. We show that periodic 71° stripe domains can be obtained in BFO film on $DyScO_3$ (DSO) substrate with SRO as the bottom electrode. In the BFO/LBFO/SRO

DOI: 10.1021/acs.nanolett.6b04512
Nano Lett. 2017, 17, 486−493

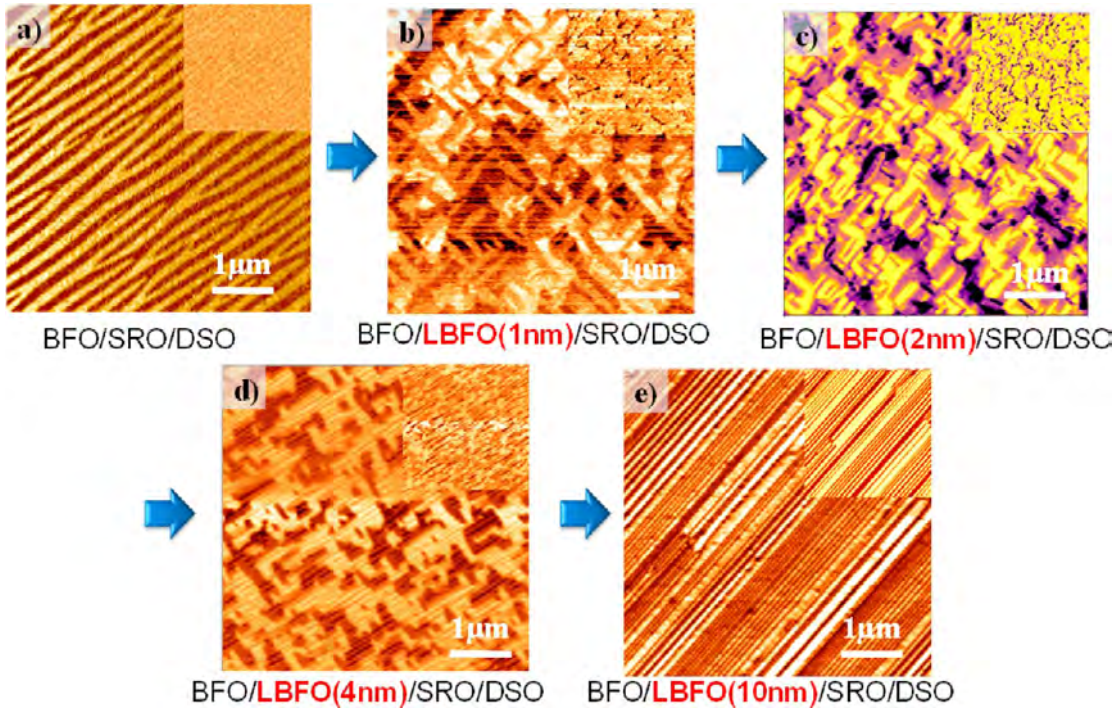

Figure 2. In-plane and out-of-plane (insets in the top right) PFM images present the domain structure evolution, with the increasing thickness of the LBFO layer, in BFO/LBFO/SRO/DSO. (a) Pure 71° domains without LBFO layer. (b–d) Mixed 71° and 109° domains exist with 1–4 nm thicknesses of the LBFO layer, and the fraction of 109° domains gradually increases according to the out-of-plane contrast. (e) Pure 109° domains with 10-nm-thick LBFO.

multilayer heterostructures, the depolarization field induced by the LBFO layer (with thickness of 1–10 nm) can gradually drive 71° stripe domains to mixed 71° and 109° domains and then to pure periodic 109° stripe domains, which has also been confirmed in the BFO/LBFO superlattices with increasing superlattice period. Furthermore, we demonstrate the origin of exchange bias in the $Co_{0.9}Fe_{0.1}$(CoFe)/BFO system through the magnetic interaction study between CoFe and BFO films with the pure 71° domain walls and pure 109° domain walls, respectively. The newly realized ability to obtain periodic 109° stripe domains with a thick SRO bottom electrode enables us to study its switching behavior and the possibility to realize electric field control of exchange bias at room temperature.

We grew a series of epitaxial 100-nm-thick BFO films, without or with 1–10 nm dielectric LBFO layer on DSO(110) substrates with 30 nm SRO as the bottom electrode by pulsed laser deposition. The heterostructure stacks are displayed as the schematics in Figure 1a. Here, the domain structure evolution from 71° domains to 109° domains by introducing a dielectric layer is predicted based on previous studies. A combination of piezoresponse force microscopy (PFM) and transmission electron microscopy (TEM) was used for the structure and ferroelectricity characterization. Magnetic properties were measured using a superconducting quantum interference device (SQUID) and the magneto-optic Kerr effect (MOKE).

The topography of the BFO/SRO/DSO sample is obtained by atomic force microscope (AFM) and is shown in Figure 1b. The atomically flat terraces, one unit cell in height, confirm the high-quality growth of the film, with a root-mean-square (RMS) roughness only of 0.2 nm. The uniform contrast of the out-of-plane PFM image (Figure 1c) and the stripe-like contrast of the in-plane image (Figure 1d) confirm the formation of periodic 71° stripe domains in BFO/SRO/DSO, which is consistent with previous work by Chu et al.[34] We introduced a thin layer (~10 nm) of LBFO between BFO and SRO, i.e., the multilayer BFO/LBFO/SRO/DSO was established. The topography (Figure 1e) also suggests the high quality of the film. Interestingly, the periodic 71° stripe domains, as shown in Figure 1c and d, are "switched" to periodic 109° domains (Figure 1f,g), which show stripe-like contrast both out-of-plane (Figure 1f) and in-plane (Figure 1g) PFM images, by inserting the LBFO layer. The key question arising here is to explore the "switching" mechanism of this phenomenon. Previous work has demonstrated that the $SrTiO_3$ dielectric layer can be used to increase the depolarization field and hence induce the monodomain to polydomain evolution in $PbTiO_3$ and $Pb(Zr,Ti)O_3$.[13,14] Here, we first time report a dielectric layer can be introduced to drive the periodic 71° stripe domains to 109° stripe domains in BFO films. We infer that the depolarization field arising from the LBFO layer plays a key role in the domain structure evolution from 71° stripe domain to periodic 109° domain in BFO.

To further understand how the LBFO layer affects the formation of domain structures in the BFO layer, a series of LBFO films with various thickness (0–10 nm) were grown between the BFO layer (~100 nm) and SRO layer (~30 nm) on DSO (110) substrate, stacking as BFO/LBFO/SRO/DSO heterostructures. Using PFM, we investigate the domain configurations of BFO in these heterostructures, focusing on the effect of the LBFO thickness in the domain structure evolution, which are displayed in Figure 2. Detailed analyses, combining of both in-plane (Figure 2a–e) and out-of-plane (insets in the top right of Figure 2a–e) PFM images of the samples with different thicknesses (0–10 nm) of LBFO layer, enable us to identify the types of ferroelectric domain walls. Here, as shown in Figure 2a–e, all of the in-plane PFM images

DOI: 10.1021/acs.nanolett.6b04512
Nano Lett. 2017, 17, 486–493

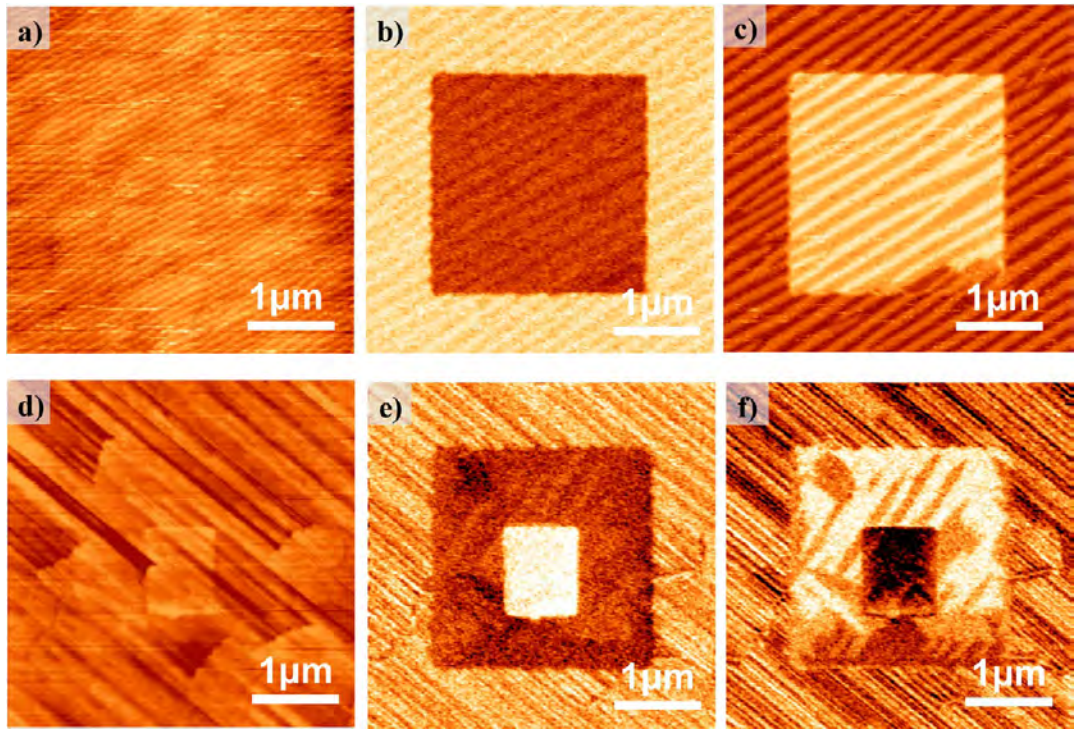

Figure 3. Switching behavior of 71° and 109° domain structures. (a) Topography, (b) out-of-plane, and (c) in-plane PFM images of BFO/SRO/DSO with 71° stripe domains after −6 V DC field poling. (d) Topography, (e) out-of-plane, and (f) in-plane PFM images of BFO/LBFO/SRO/DSO with 109° stripe domains after −6 and 6 V DC field poling.

show stripe-like contrast; thus the uniform out-of-plane contrast presents the pure 71° domain walls while the existence of black contrast in the out-of-plane images implies the presence of 109° domain walls. It is revealed that pure 71° stripe domains without LBFO layer (Figure 2a) gradually evolve to mixed 71° and 109° domain structures, where the fraction of 109° domains (which can be identified from the out-of-plane image contrast) gradually increases with the increasing thickness of LBFO from 1 to 4 nm (Figure 2b–d) and finally turns into pure 109° stripe domain walls with 10-nm-thick LBFO (Figure 2e). We also studied the effect of thicker LBFO layer (as thick as 50 nm) on the domain structure evolution which is still a periodic 109° stripe domain structure.

Based on the PFM data in Figure 1 and Figure 2, we can now better understand the role played by LBFO layer in controlling the domain structures in the BFO layer. In the BFO/SRO/DSO stack (without LBFO), the screening effects at the ferroelectric(BFO)/metal(SRO) interface enable the formation of 71° domains, while the introduction of the LBFO dielectric space layer enables the increase of the distance between the screening charges from the SRO and BFO, leading to the reduction of the screening effects and hence the increase of the depolarization field. Consequently, the 71° stripe domain is destabilized, and the 109° stripe domain structure forms to decrease the energy cost owing to the strong depolarization field. Therefore, through tuning the thickness of the LBFO layer, the depolarization field can be manipulated to design and control the domain configuration of BFO film.

The ability to accurately control the 71° and 109° stripe domains, demonstrated in this Letter, enables us to study the switching behavior of these domain structures, which is essential for exploiting the domain wall functionality and magnetoelectric device applications. A previous study has demonstrated the formation of 109° stripe domains with insertion of a ultrathin SRO bottom electrode; however, it is very difficult to switch due to the high room temperature resistivity of SRO, ∼3 mΩ cm at a thickness of 4 nm.[34] In this study, periodic 109° stripe domains were obtained by inserting a LBFO layer with the presence of 30-nm-thick SRO bottom electrode, enabling us to study the switching behavior for the first time. Figure 3 shows the topography, out-of-plane, and in-plane PFM images of the samples after applying a DC electric field. Distinct switching behaviors are observed in the films with different domain structures. As shown in Figure 3a–c, it is revealed that periodic 71° stripe domains in the BFO/SRO/DSO heterostructure can be switched back and forth after the −6 V field poling, which is in agreement with earlier study.[33] The reversible switching of 71° domains has stimulated the study of electric field control of magnetism in the ferromagnet/mutiferroic BFO heterostructures.[26]

Recently, strong exchange bias has been reported in the ferromagnet/mutiferroic BFO system with mosaic domain structures (comprising a large fraction of 109° domain walls),[36] opening a new possibility to realize the electric field control of exchange bias. However, Allibe et al.[25] reported that the exchange bias cannot be reversibly manipulated by the electric field in a CoFeB/BFO (with mosaic domains) based spin valve. The switching behavior study of 109° stripe domains may help to understand the reason why the exchange bias is not reversibly switched using the electric field. According to the topography, out-of-plane, and in-plane PFM images in Figure 3d–f, we find that the periodic 109° stripe domains are predominately switched to 71° or single domain after applying −6 and 6 V DC field. Therefore, the 109° stripe domains cannot be switched back and forth, leading to the decline of exchange bias in the previous study. A detailed study of the

DOI: 10.1021/acs.nanolett.6b04512
Nano Lett. 2017, 17, 486–493

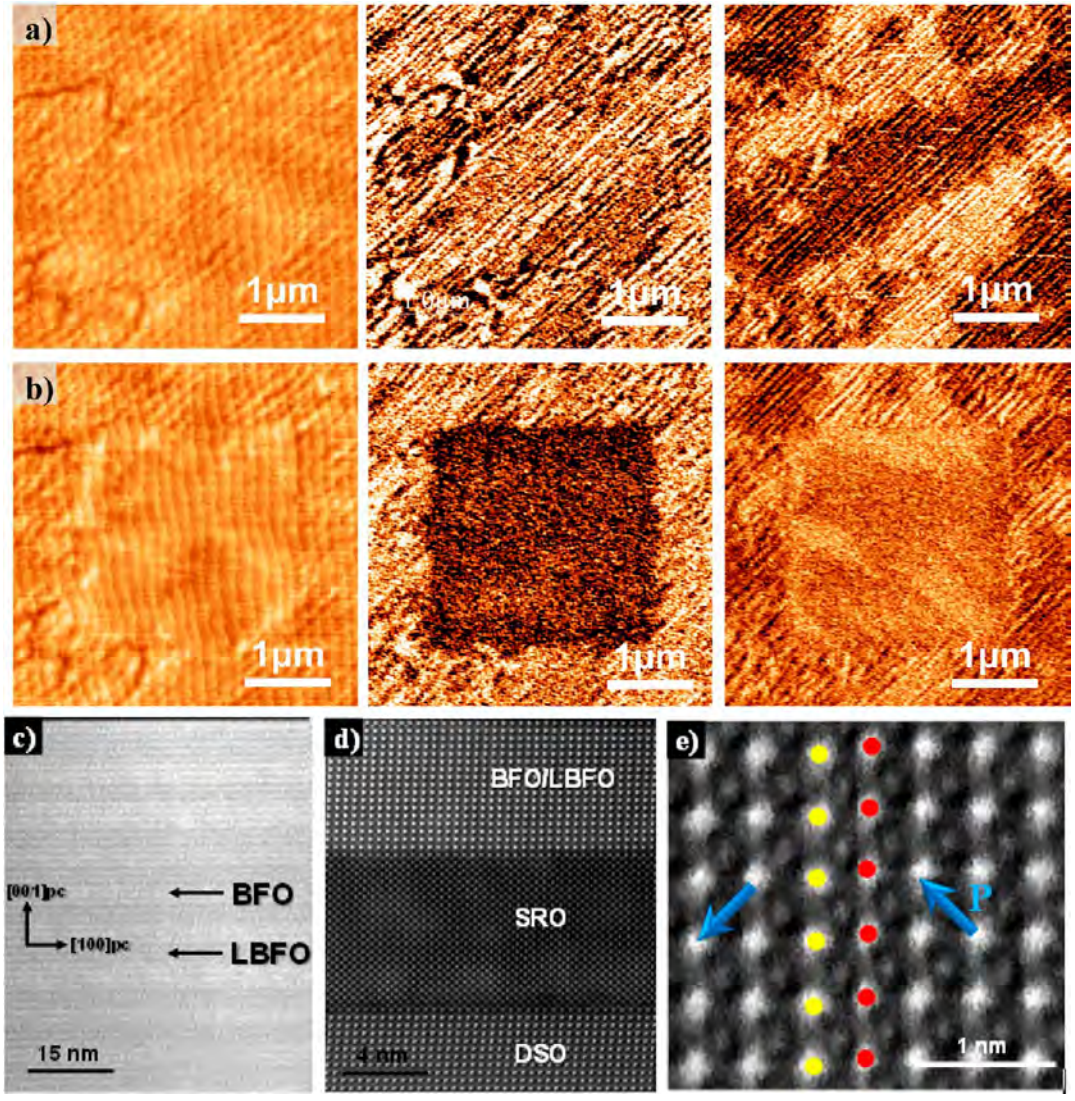

Figure 4. Topography, out-of-plane, and in-plane PFM images (from left to right) of 10 × 10 BFO/LBFO superlattices: (a) Periodic 109° domain walls in the as-grown 10 × 10 BFO/LBFO superlattices. (b) Switching behavior of 109° domains poled with a −6 V DC field. STEM images of BFO/LBFO superlattices: (c) A low-magnification cross-sectional image of the 10 × 10 BFO/LBFO superlattices. (d) High-resolution STEM image of SRO/DSO and BFO/SRO interfaces. (e) HAADF STEM image shows the 109° domain walls in 10 × 10 BFO/LBFO superlattices.

switching behavior of 109° domain structure with the increasing poling DC field from 1 to 9 V is shown in Figure S1. It further confirms that, by applying a DC voltage on the film, we can effectively "erase" areas of 109° domain walls. 109° stripe domains have a common in-plane polarization (100 or 010) but oscillate out-of-plane polarization. Thus, a singular out-of-plane polarization will be created with an applied voltage, making it 71° domains or even single domain. The important topic of how to switch 109° stripe domains back and forth is still under further study, which is critical for achieving the room temperature electric field reversible control of exchange bias.[29]

After successfully realizing the depolarization field driven domain structure evolution in BFO films, we next try to extend this interface engineering effect to BFO/LBFO superlattices. Symmetric (BFO)n/(LBFO)n superlattices with n = 3, 10, and 20 were synthesized on DSO (110) substrates via pulsed-laser deposition. Here, superlattices are referred to using the "$n \times n$" shorthand wherein n corresponds to the thickness of the BFO and LBFO layers in unit cells. As shown in Figure S2, Figure 4a,b, and Figure S3, the topography, out-of-plane, and in-plane PFM images of the 3 × 3, 10 × 10, and 20 × 20 BFO/LBFO samples are displayed from left to right. It is found that the PFM images of 3 × 3 (Figure S2a) BFO/LBFO superlattices show mixed 71° and 109° domain structures, while 10 × 10 (Figure 4a) and 20 × 20 (Figure S3a) superlattices possess periodic 109° stripe domains, implying the interface engineering of domain structure evolution in the BFO/LBFO superlattices with increasing superlattice period, as a thicker LBFO layer can produce a larger depolarization field. The switching behaviors of these superlattices are also studied (displayed in Figure S2b, Figure 4b, and Figure S3b), it further confirms that the 109° domains are switched to 71° domains or single domain.

A typical low-magnification cross-sectional image of the BFO/LBFO superlattices is shown in Figure 4c taken by high-angle annular dark field (HAADF) scanning transmission electron microscopy (STEM). The image confirms the BFO/LBFO superlattices have high quality epitaxial growth, revealing the layer uniformity with sharp BFO/LBFO interfaces. A high-

DOI: 10.1021/acs.nanolett.6b04512
Nano Lett. 2017, 17, 486−493

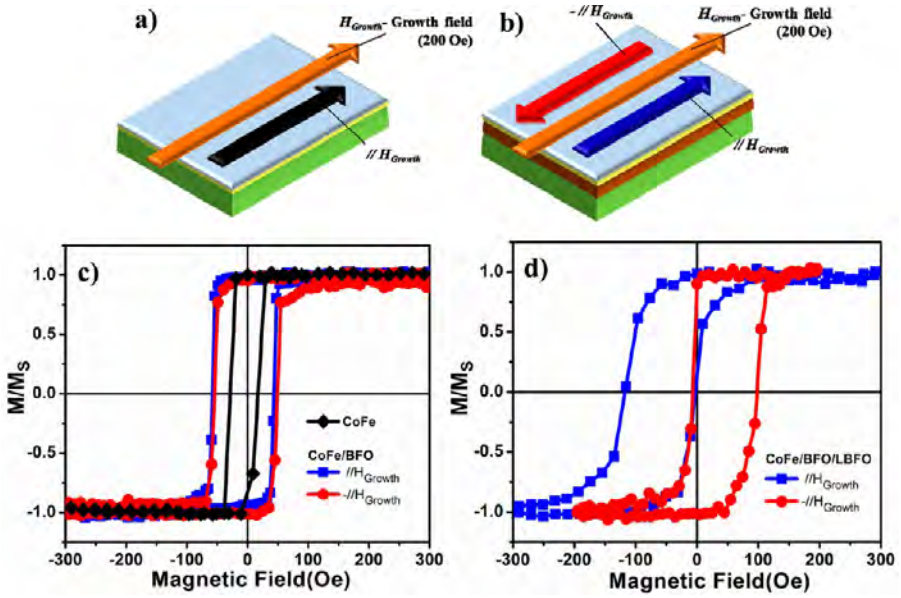

Figure 5. Schematics of the applied magnetic growth field (200 Oe) orientation during CoFe growth and the direction of the magnetic field during the SQUID measurement of (a) Pt/CoFe/DSO and (b) Pt/CoFe/BFO/DSO or Pt/CoFe/BFO/LBFO/DSO. (c) Magnetic properties of Pt/CoFe (black loop) and CoFe/BFO (pure 71° domain wall) demonstrate the exchange enhancement due to the exchange coupling between CoFe and BFO. (d) Magnetic interactions in CoFe/BFO/LBFO (pure 109° domain wall) reveal both the exchange enhancement and the exchange bias.

resolution *Z*-contrast image of the SRO/DSO and BFO/SRO interfaces is shown in Figure 4d, illustrating the atomic-scale epitaxy between the SRO and DSO substrate and (L)BFO/SRO layers. As shown in Figure 4c, the bright layers are the BFO layer, and the dark layers are LBFO; the sharp BFO/LBFO interface can be identified. However, the interface of BFO/LBFO cannot be identified in this high-resolution STEM image (Figure 4d) because the compositions of the two layers are not sufficiently distinguished. The HAADF STEM image displayed in Figure 4e and the dark field cross-sectional TEM image shown in Figure S4 further confirms that the 109° domain walls are obtained in BFO/LBFO superlattices, which is consistent with the PFM data in Figure 4a.

We next turn to the study of magnetic interactions in the Pt/CoFe/BFO heterostructures. CoFe (2.5 nm) and Pt (2.5 nm) layers were deposited on BFO/SRO/DSO (with pure periodic 71° domain walls) and BFO/LBFO/SRO/DSO samples (with pure periodic 109° domain walls) via DC magnetron sputtering, respectively. CoFe and Pt were also deposited directly to the DSO substrates to compare the behavior of the Pt/CoFe/DSO stack to the Pt/CoFe/BFO/SRO/DSO and Pt/CoFe/BFO/LBFO/SRO/DSO stacks. The growth of the CoFe layer was completed in an applied magnetic field of 200 Oe (H_{Growth}) to induce unidirectional anisotropy in the CoFe/BFO heterostructures. In this study, the growth field of CoFe was applied perpendicular to the 71° or 109° domain walls. Figure 5a,b provides a schematic illustration to explain the orientation of applied magnetic growth field and the direction of the magnetic field during the SQUID measurement. It is important to note that two distinctly different types of behavior are found. In Figure 5c, a SQUID measurement parallel to H_{Growth} shows very small Hc (~10−15 Oe) with almost no shift of the M−H loop in the Pt/CoFe/DSO stack. Only the exchange enhancement (H_C~ 50 Oe) is observed (Figure 5c) in the CoFe/BFO system with 71° domain walls (consistent with the previous work[39]), while the CoFe/BFO/LBFO sample with 109° domain walls, as shown in Figure 5d, exhibits both a strong exchange bias (typical $|H_{EB}|$ ~ 50 Oe) and significant enhancement of H_C (H_C ~ 50 Oe). Confirmation of such exchange bias interaction is obtained upon 180° rotation of the samples, where one can observe the opposite shift of the hysteresis loop when measured antiparallel to H_{Growth} (the blue M−H loop in Figure 5d). The exchange bias in CoFe/BFO/LBFO has also been confirmed via MOKE measurement (Figure S5). In the BFO mosaic domain structures, a previous study has demonstrated that 109° domain walls can play an important role in determining the exchange bias in CoFe/BFO system.[25,36] Here, the precise controlling of pure 71° and 109° periodic stripe domain walls enable us to make a clear demonstration that the exchange bias in the CoFe/BFO system originates from the pinned, uncompensated spins at 109° domain walls in BFO.

In summary, our studies have revealed the ability to precisely control the domain structure by tuning the depolarization field with a dielectric layer in multilayer BFO/LBFO/SRO/DSO heterostructures. This interface effect has also been successfully extended to the BFO/LBFO superlattices. Furthermore, the 109° stripe domain structures with SRO bottom electrode enable us to study the switching behavior for the first time. We also report that a clear demonstration of the origin of exchange bias in CoFe/BFO system is from the 109° domain walls. These findings provide future directions to study an electric field control of exchange bias and open a new pathway to explore the room temperature multiferroic vortices in multiferroic BFO system such as BFO/LBFO superlattices.

■ ASSOCIATED CONTENT

Supporting Information

The Supporting Information is available free of charge on the ACS Publications website at DOI: 10.1021/acs.nanolett.6b04512.

Experimental details and Figures S1−S5 (PDF)

DOI: 10.1021/acs.nanolett.6b04512
Nano Lett. 2017, 17, 486−493

AUTHOR INFORMATION

Corresponding Authors

*E-mail: dychen1987@gmail.com.
*E-mail: xingsengao@scnu.edu.cn.
*E-mail: medczeng@scut.edu.cn.

ORCID

Deyang Chen: 0000-0002-8370-6409

Author Contributions

D.Y.C. and Z.H.C. contributed equally to this work.

Notes

The authors declare no competing financial interest.

ACKNOWLEDGMENTS

We sincerely thank Professor Ramamoorthy Ramesh for the fruitful discussions and suggestions. The work was supported by the National Key Research and Development Program of China (No. 2016YFA0201002), the National Science Foundation (Nanosystems Engineering Research Center for Translational Applications of Nanoscale Multiferroic Systems) under grant number EEC-1160504, and the NSF Center for Energy Efficient Electronics Science (E^3S) under grant number ECCS-0939514. Electron microscopy work (Q.H. and A.Y.B.) was supported by the U.S. Department of Energy (DOE) Office of Science, Office of Basic Energy Sciences (BES), Materials Science and Engineering Division. This work was also supported by NSFC (Grant Nos. 51431006, 11474146, 61674062, 51602110). D.Y.C. acknowledges the scholarship from Oversea Study Program of Guangzhou Elite Project (GEP). X.S.G. acknowledges the Project for Guangdong Province Universities and Colleges Pearl River Scholar Funded Scheme (2014), and D.C.Z. acknowledges the support from Science and Technology Program of Guangzhou (2016201604030070).

REFERENCES

(1) Mannhart, J.; Schlom, D. G. *Science* **2010**, *327*, 1607−1611.
(2) Hwang, H. Y.; Iwasa, Y.; Kawasaki, M.; Keimer, B.; Nagaosa, N.; Tokura, Y. *Nat. Mater.* **2012**, *11*, 103−113.
(3) Mundy, J. A.; Brooks, C. M.; Holtz, M. E.; Moyer, J. A.; Das, H.; Rébola, A. F.; Heron, J. T.; Clarkson, J. D.; Disseler, S. M.; Liu, Z.; Farhan, A.; Held, R.; Hovden, R.; Padgett, E.; Mao, Q.; Paik, H.; Misra, R.; Kourkoutis, L. F.; Arenholz, E.; Scholl, A.; Borchers, J. A.; Ratcliff, W. D.; Ramesh, R.; Fennie, C. J.; Schiffer, P.; Muller, D. A.; Schlom, D. G. *Nature* **2016**, *537*, 523−527.
(4) Zubko, P.; Gariglio, S.; Gabay, M.; Ghosez, P.; Triscone, J.-M. *Annu. Rev. Condens. Matter Phys.* **2011**, *2*, 141−165.
(5) Dong, S.; Liu, J.-M.; Cheong, S.-W.; Ren, Z. *Adv. Phys.* **2015**, *64*, 519−626.
(6) Stengel, M.; Vanderbilt, D.; Spaldin, N. A. *Nat. Mater.* **2009**, *8*, 392−397.
(7) Yu, P.; Chu, Y.-H.; Ramesh, R. *Mater. Today* **2012**, *15*, 320−327.
(8) Bousquet, E.; Dawber, M.; Stucki, N.; Lichtensteiger, C.; Hermet, P.; Gariglio, S.; Triscone, J. M.; Ghosez, P. *Nature* **2008**, *452*, 732−736.
(9) Tang, Y. L.; Zhu, Y. L.; Ma, X. L.; Borisevich, A. Y.; Morozovska, A. N.; Eliseev, E. A.; Wang, W. Y.; Wang, Y. J.; Xu, Y. B.; Zhang, Z. D.; Pennycook, S. J. *Science* **2015**, *348*, 547−551.
(10) Yadav, A. K.; Nelson, C. T.; Hsu, S. L.; Hong, Z.; Clarkson, J. D.; Schlepuetz, C. M.; Damodaran, A. R.; Shafer, P.; Arenholz, E.; Dedon, L. R.; Chen, D.; Vishwanath, A.; Minor, A. M.; Chen, L. Q.; Scott, J. F.; Martin, L. W.; Ramesh, R. *Nature* **2016**, *530*, 198−201.
(11) Kim, D. J.; Jo, J. Y.; Kim, Y. S.; Chang, Y. J.; Lee, J. S.; Yoon, J.-G.; Song, T. K.; Noh, T. W. *Phys. Rev. Lett.* **2005**, *95*, 237602.
(12) Lu, H.; Liu, X.; Burton, J. D.; Bark, C. W.; Wang, Y.; Zhang, Y.; Kim, D. J.; Stamm, A.; Lukashev, P.; Felker, D. A.; Folkman, C. M.; Gao, P.; Rzchowski, M. S.; Pan, X. Q.; Eom, C. B.; Tsymbal, E. Y.; Gruverman, A. *Adv. Mater.* **2012**, *24*, 1209−1216.
(13) Lichtensteiger, C.; Fernandez-Pena, S.; Weymann, C.; Zubko, P.; Triscone, J. M. *Nano Lett.* **2014**, *14*, 4205−4211.
(14) Liu, G.; Chen, J.; Lichtensteiger, C.; Triscone, J.-M.; Aguado-Puente, P.; Junquera, J.; Valanoor, N. *Adv. Electron. Mater.* **2016**, *2*, 1500288.
(15) Wang, J.; Neaton, J. B.; Zheng, H.; Nagarajan, V.; Ogale, S. B.; Liu, B.; Viehland, D.; Vaithyanathan, V.; Schlom, D. G.; Waghmare, U. V.; Spaldin, N. A.; Rabe, K. M.; Wuttig, M.; Ramesh, R. *Science* **2003**, *299*, 1719−1722.
(16) Streiffer, S. K.; Parker, C. B.; Romanov, A. E.; Lefevre, M. J.; Zhao, L.; Speck, J. S.; Pompe, W.; Foster, C. M.; Bai, G. R. *J. Appl. Phys.* **1998**, *83*, 2742.
(17) Seidel, J.; Martin, L. W.; He, Q.; Zhan, Q.; Chu, Y. H.; Rother, A.; Hawkridge, M. E.; Maksymovych, P.; Yu, P.; Gajek, M.; Balke, N.; Kalinin, S. V.; Gemming, S.; Wang, F.; Catalan, G.; Scott, J. F.; Spaldin, N. A.; Orenstein, J.; Ramesh, R. *Nat. Mater.* **2009**, *8*, 229−234.
(18) Balke, N.; Winchester, B.; Ren, W.; Chu, Y. H.; Morozovska, A. N.; Eliseev, E. A.; Huijben, M.; Vasudevan, R. K.; Maksymovych, P.; Britson, J.; Jesse, S.; Kornev, I.; Ramesh, R.; Bellaiche, L.; Chen, L. Q.; Kalinin, S. V. *Nat. Phys.* **2011**, *8*, 81−88.
(19) Choi, T.; Lee, S.; Choi, Y.; Kiryukhin, V.; Cheong, S.-W. *Science* **2009**, *324*, 63−66.
(20) Yang, S. Y.; Seidel, J.; Byrnes, S. J.; Shafer, P.; Yang, C. H.; Rossell, M. D.; Yu, P.; Chu, Y. H.; Scott, J. F.; Ager, J. W., III; Martin, L. W.; Ramesh, R. *Nat. Nanotechnol.* **2010**, *5*, 143.
(21) Guo, R.; You, L.; Chen, L.; Wu, D.; Wang, J. *Appl. Phys. Lett.* **2011**, *99*, 122902.
(22) Bhatnagar, A.; Roy Chaudhuri, A.; Heon Kim, Y.; Hesse, D.; Alexe, M. *Nat. Commun.* **2013**, *4*, 2835.
(23) Zhao, T.; Scholl, A.; Zavaliche, F.; Lee, K.; Barry, M.; Doran, A.; Cruz, M. P.; Chu, Y. H.; Ederer, C.; Spaldin, N. A.; Das, R. R.; Kim, D. M.; Baek, S. H.; Eom, C. B.; Ramesh, R. *Nat. Mater.* **2006**, *5*, 823−829.
(24) Chu, Y. H.; Martin, L. W.; Holcomb, M. B.; Gajek, M.; Han, S.-J.; He, Q.; Balke, N.; Yang, C.-H.; Lee, D.; Hu, W.; Zhan, Q.; Yang, P.-L.; Fraile-Rodriguez, A.; Scholl, A.; Wang, S. X.; Ramesh, R. *Nat. Mater.* **2008**, *7*, 478−482.
(25) Allibe, J.; Fusil, S.; Bouzehouane, K.; Daumont, C.; Sando, D.; Jacquet, E.; Deranlot, C.; Bibes, M.; Barthélémy, A. *Nano Lett.* **2012**, *12*, 1141−1145.
(26) Heron, J. T.; Bosse, J. L.; He, Q.; Gao, Y.; Trassin, M.; Ye, L.; Clarkson, J. D.; Wang, C.; Liu, J.; Salahuddin, S.; Ralph, D. C.; Schlom, D. G.; Iniguez, J.; Huey, B. D.; Ramesh, R. *Nature* **2014**, *516*, 370−373.
(27) Lubk, A.; Gemming, S.; Spaldin, N. A. *Phys. Rev. B: Condens. Matter Mater. Phys.* **2009**, *80*, 104110.
(28) He, Q.; Yeh, C. H.; Yang, J. C.; Singh-Bhalla, G.; Liang, C. W.; Chiu, P. W.; Catalan, G.; Martin, L. W.; Chu, Y. H.; Scott, J. F.; Ramesh, R. *Phys. Rev. Lett.* **2012**, *108*, 067203.
(29) Chen, D.; Gao, X.; Liu, J.-M. *MRS Commun.*, 10.1557/mrc.2016.39.
(30) Catalan, G.; Seidel, J.; Ramesh, R.; Scott, J. F. *Rev. Mod. Phys.* **2012**, *84*, 119−156.
(31) Sando, D.; Barthélémy, A.; Bibes, M. *J. Phys.: Condens. Matter* **2014**, *26*, 473201.
(32) Tian, G.; Zhang, F. Y.; Yao, J. X.; Fan, H.; Li, P. L.; Li, Z. W.; Song, X.; Zhang, X. Y.; Qin, M. H.; Zeng, M.; Zhang, Z.; Yao, J. J.; Gao, X. S.; Liu, J. M. *ACS Nano* **2016**, *10*, 1025−1032.
(33) Chu, Y.-H.; Zhan, Q.; Martin, L. W.; Cruz, M. P.; Yang, P.-L.; Pabst, G. W.; Zavaliche, F.; Yang, S.-Y.; Zhang, J.-X.; Chen, L.-Q.; Schlom, D. G.; Lin, I. N.; Wu, T.-B.; Ramesh, R. *Adv. Mater.* **2006**, *18*, 2307−2311.
(34) Chu, Y.-H.; He, Q.; Yang, C.-H.; Yu, P.; Martin, L. W.; Shafer, P.; Ramesh, R. *Nano Lett.* **2009**, *9*, 1726−1730.

DOI: 10.1021/acs.nanolett.6b04512
Nano Lett. 2017, 17, 486−493

(35) Chen, Z.; Liu, J.; Qi, Y.; Chen, D.; Hsu, S.-L.; Damodaran, A. R.; He, X.; N'Diaye, A. T.; Rockett, A.; Martin, L. W. *Nano Lett.* **2015**, *15*, 6506−6513.
(36) Martin, L. W.; Chu, Y. H.; Holcomb, M. B.; Huijben, M.; Yu, P.; Han, S. J.; Lee, D.; Wang, S. X.; Ramesh, R. *Nano Lett.* **2008**, *8*, 2050−2055.
(37) Zhang, Q.; Zhu, X. H.; Xu, Y. H.; Gao, H. B.; Xiao, Y. J.; Liang, D. Y.; Zhu, J. L.; Zhu, J. G.; Xiao, D. Q. *J. Alloys Compd.* **2013**, *546*, 57−62.
(38) Cheng, C.-J.; Kan, D.; Anbusathaiah, V.; Takeuchi, I.; Nagarajan, V. *Appl. Phys. Lett.* **2010**, *97*, 212905.
(39) Heron, J. T.; Trassin, M.; Ashraf, K.; Gajek, M.; He, Q.; Yang, S. Y.; Nikonov, D. E.; Chu, Y. H.; Salahuddin, S.; Ramesh, R. *Phys. Rev. Lett.* **2011**, *107*, 217202.

DOI: 10.1021/acs.nanolett.6b04512
Nano Lett. 2017, 17, 486−493